International Journal of Mechanical, Industrial and Aerospace Sciences
ISSN: 2517-9950
Vol:5, No:7, 2011

Investigations of Free-to-Roll Motions and its Active Control under Pitch-up Maneuvers

Tanveer A. Khan, Xue Y. Deng, Yan K. Wang, Xu Si-Wen

***Abstract*—**Experiments have been carried out at sub-critical Reynolds number to investigate free-to-roll motions induced by forebody and/or wings complex flow on a 30° swept back non-slender wings-slender body-model for static and dynamic (pitch-up) cases. For the dynamic (pitch-up) case it has been observed that roll amplitude decreases and lag increases with increase in pitching speed. Decrease in roll amplitude with increase in pitch rate is attributed to low disturbing rolling moment due to weaker interaction between forebody and wing flow components. Asymmetric forebody vortices dominate and control the roll motion of the model in dynamic case when non-dimensional pitch rate $\geq 1x10^{-2}$. Effectiveness of the active control scheme utilizing rotating nose with artificial tip perturbation is observed to be low in the angle of attack region where the complex flow over the wings has contributions from both forebody and wings.

***Keywords*—**Artificial Tip Perturbation, Experimental Investigations, Forebody Asymmetric Vortices, Non-slender Wings-Body Model, Wing Rock

I. INTRODUCTION

WING rock on high swept wings and body configurations at high angles of attack has been comprehensively reviewed by Katz [1] and Nelson [2]. Brandon and Nguyen [3] found in experiments that even with very low sweep wings a generic wing body model could also produce a "wing rock" motion at high angles of attack. The forebody-induced wing rock was also found in subscale experiments for F-18 HARV [4], X-31 [5] and other generic wing body models [6]-[8]. It has long been recognized that the forebody vortices over a slender forebody will become asymmetric at high angles of attack, even at no sideslip. Therefore it is speculated that the asymmetric vortex flow could be relevant to the wing rock on a wing body model. Deng, Chen and co-workers [9]-[10] concluded in their research that the non-determinacy of the asymmetric vortices flow is caused by the non-determinacy of micro irregular disturbances on model nose from the machining tolerances instead of asymmetric vortices flow itself and asymmetric vortices flow should be determinate in nature. Using an artificial mini-perturbation on the nose makes the asymmetric vortices flow repeatable and deterministic without inducing any fundamental change in its characteristics. Forebody asymmetric vortices resulting in roll-oscillations may be controlled or reduced through switching of the vortices by rotating the nose tip [11]. Gursul et al [12] reviewed flow structures and aerodynamics of non-slender wings. Vortical flows develop at very low angles of attack, and form close to the wing surface. Three distinct stages were identified in the break down process [13]: small scale undulations of the vortex core filament, onset of vortex breakdown and abrupt expansion of the breakdown region. Vortex breakdown is observed to be much less abrupt compared to breakdown over slender wings. One of the distinct features of non-slender wings is the location of the primary attachment zone outboard of the symmetry plane. Unusual self-excited roll oscillations have also been observed for free-to-roll non-slender wings for a lower sweep angle of Λ=45° [14]. These oscillations were observed around the stall angle, where the reattachment of asymmetric flows was the most important factor. These initial experiments and the related ongoing work on non-slender wings suggested that the main cause of these self-excited oscillations was the separated and vortical flows, which could be very different from those for slender wings. In particular, the flow reattachment is suspected to play an important role in the unsteady aerodynamics.Most of the work done in the past on wing rock has been focused on high swept wings or slender wings and body configurations. As a result low sweep wings and low sweep wing-body configurations have received little attention. Little work done on the non-slender wings had also been related to low angles of attack only. Additionally, past studies have been focused mainly on free-to-roll (FTR) only models. This study is focused on understanding the flow structures and related aerodynamics of a low-sweep wing-slender body configuration undergoing self-excited rolling motions at static angles of attack, $0° \leq \alpha \leq 90°$, and also undergoing large amplitude pitch-up motions at sub-critical Reynolds number covering a wide range of angles of attack. Effects of pitch-up motions at variable rates on the roll characteristics of the model under consideration have also been investigated. Effectiveness of the active control technique utilizing rotating nose tip with artificial perturbation on a FTR model undergoing pitch-up motions at variable rates would also be investigated.

II. EXPERIMENTAL SETUP

Two models, similar in geometry, were used for the experiments. Free-to-roll (FTR) model, Fig. 1 (a), was used to record time histories of FTR motion. Forced-to-roll model,

Tanveer A. Khan is PhD Candidate; (e-mail: tkhan@syr.edu).
Xue Y. Deng is senior Professor; (e-mail: dengxueying@vip.sina.com).
Yan K. Wang is a Professor; (e-mail: wangyankui@buaa.edu.cn).
Xu Si-Wen is PhD Candidate; (e-mail: mist1987@163.com).

All authors are affiliated with Institute of Fluid Mechanics, Beihang University, Beijing, 100191 P. R. China

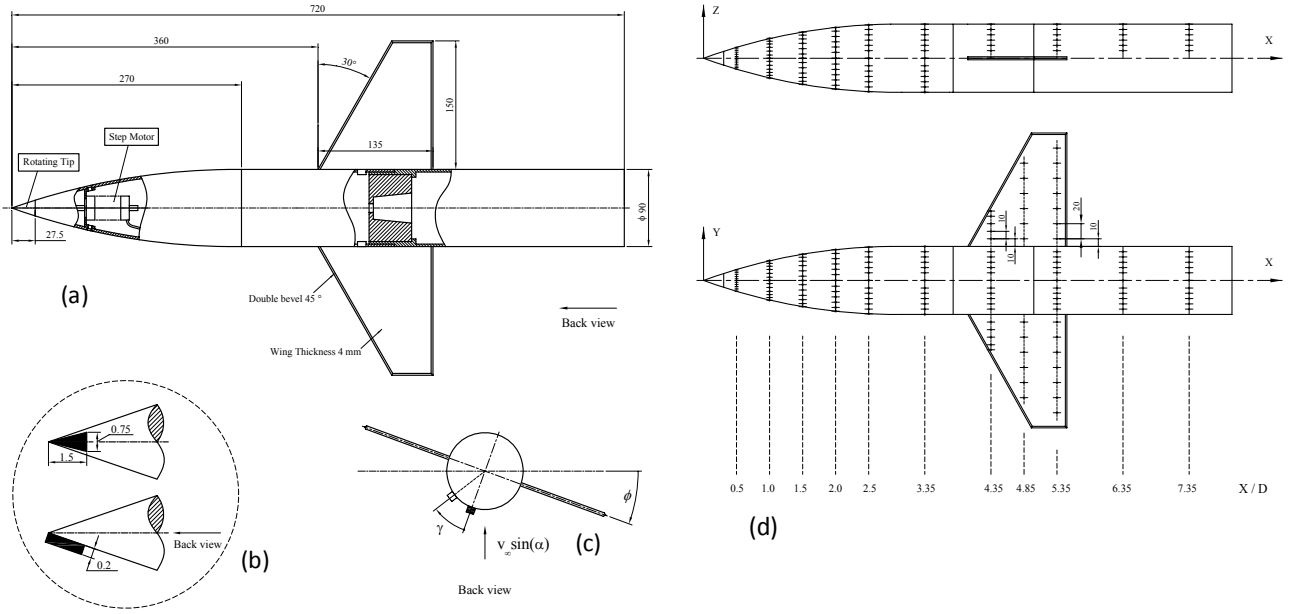

Fig. 1 (a) Free-to-roll model, dimensions in mm (b) Mini perturbation (sphere or delta block) on the model nose (c) Change in rotational angle of the mini-perturbation in wind-axis system with roll angle (d) Forced-to-roll model showing locations of pressure taps and sections.

exactly similar in geometry, has number of surface pressure measurement taps and was driven by a servomotor playing back the FTR time histories, Fig. 1 (d). Purpose of using two models was to acquire FTR time histories independent of any obstruction from pressure tubing. Both models include a slender body with a rotating nose having artificial mini-perturbation on it and low sweep wings with 30° sweep angle. The rotational angle, γ, of the tip perturbation around a body is defined in a body axis system and the clockwise rotation is positive from the rear view of the model. γ=0° is located at the vertical symmetry plane of the lower surface of the model. The rotational angle of the nose in a wind axis system equals the γ plus the model rolling angle φ, as shown in Fig. 1 (c). The body diameter D equals 90 mm and the nose is pointed-ogive and tangent with a cylindrical afterbody. All measurements reported in this paper were taken at zero side-slip and at experimental Reynolds number of 1.6×10^5 based on the cylinder diameter, unless mentioned otherwise. Pressure Systems Inc. DTC miniature ESP pressure scanners and Dantec Dynamics PIV system were used for unsteady surface pressure and vortex wake measurements respectively. Synchronous and phase-locked measurements of these were possible using a triggering system. Angular resolution in roll and pitch were computed as 0.0879° and 0.045° respectively. Pressure tubing used in experiments was not more than 1 meter long as the pressure amplitude error will not be more than 1% and the pressure phase error will not be more than 3% for unsteady measurements. Uncertainty in pressure coefficient, cp was found to be less than 1% of maximum cp.

III. Results and Discussions

In order to understand the effect of pitch rate on the roll behavior it is believed that insight into the roll oscillations and corresponding flow features at static angles of attack, α, is essential. FTR motion and corresponding flow and aerodynamics characteristics at static angles of attack shall be discussed first followed by the description of effect of pitch rate and active control effectiveness in the dynamic case.

A. Static-α Results

1. FTR Motion Analysis

Different roll behavior at different α was observed in free-to-roll, FTR, measurements. Fig. 2 presents summary of FTR motion at static alphas for 3 different positions of tip perturbation, γ=45°, -45° & 0°.

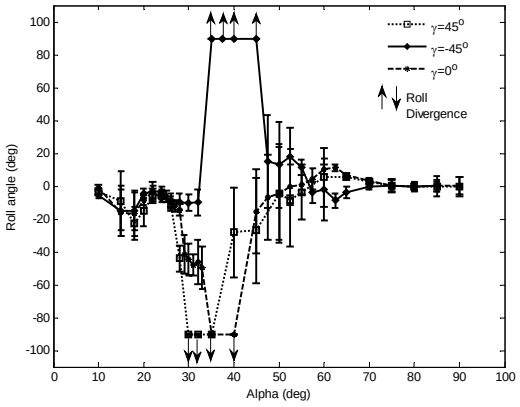

Fig. 2 Summary of FTR motion at static alphas for 3 different positions of tip perturbation, γ=45°, -45° & 0°.Error bars showing standard deviation of roll angle, φ

Error bars show standard deviation of roll angle φ, roll divergence indicates turn-around of the model and the markers represent mean roll angle in Fig. 2. For $10° \le \alpha \le 26°$ similar FTR motion for all three γ implies that there is no significant effect of γ on the roll behavior indicating absence of any

forebody asymmetric vortices as these are found to be sensitive to γ, [9]. Hence, Small roll oscillations at non-zero trim roll angles are only due to the asymmetry in wings flow components in this region that will be called as wings induced roll region. It has also been shown that bubble burst region over wings of 30° sweep angle extends from 12° < α < 42° [15] suggesting presence of some contribution from the wings flow components till α ≈ 42°. Hence, wings-body interaction roll region is defined extending from 26° < α ≤ 45°. It may be noted that in this region phenomenon of roll divergence occurs from α = 30° to 45° for various tip perturbation positions. In this α range when the model's brake is released to set off FTR motion it rolls to one side and turns around. This roll divergence is rapid when 30° ≤ α ≤ 40° and gradual when 40° < α ≤ 45°. The model builds up roll oscillations and diverges after few oscillations in gradual divergence contrary to sudden divergence without any oscillation in the other case. Forebody asymmetric vortices and resulting side force on the body sections have been witnessed till α = 70°, [16], and the roll oscillations encountered in the region 45° ≤ α ≤ 70° are believed to be due to the asymmetric forebody vortices and the region is characterized as forebody induced roll region. For 70° < α ≤ 90° slight roll oscillations are believed to be due to the unsteady effects caused by random wake shedding [16]. Fig. 3 presents the characterization of angles of attack regions based on FTR motion characteristics and dominant source of asymmetry causing roll oscillations.

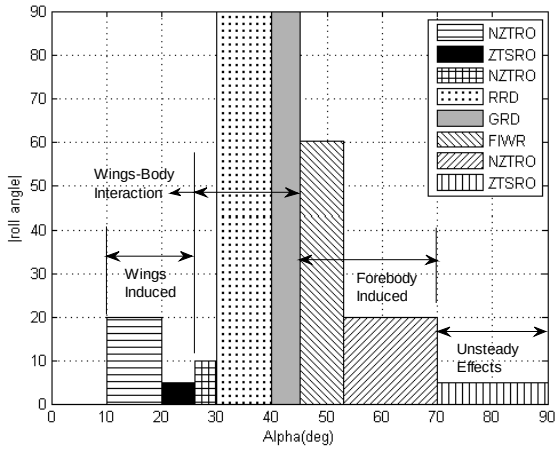

Fig. 3 Characterization of angle of attack regions based on roll motion characteristics and dominant source of asymmetry

NZTRO : Non-zero trim angle roll oscillations, ZTSRO : Zero trim angle small roll oscillations, RRD : Rapid roll divergence , GRD: Gradual roll divergence, FIWR : Forebody induced wing rock

2. Wings Induced Roll Region

In the wings induced roll region small suction peaks on wing section at α =8° & 10° were observed indicating presence of leading edge bubble or vortices but, not as strong as in case of high swept wings. Fig. 4 represents pressure coefficient c_p distributions at wing section x/D=4.85 for various angles of attack. Inboard movement of pressure peaks (and the re-attachment points) may be noticed as α changes from 8° to 10°. This may be due to the bubble extension phenomenon, [15] and it may also be observed that pressure distributions on the two wings are quite symmetric for these α. Change in the flow structure due to bubble burst for α > 10° is quite evident from Fig. 4. Slight asymmetry in the pressure distributions on left and right wings can be noticed and therefore, it is believed that asymmetry in bubble burst for α > 10° is responsible for the initial disturbing rolling moment.

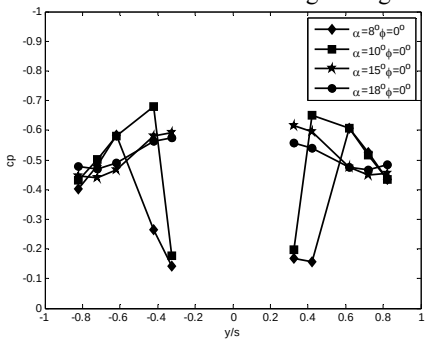

Fig. 4 Upper surface c_p distributions for various α at x/D=4.85 (wing section), s: semi-span

Fig. 5 presents variation of total rolling moment coefficient, C_l with roll angle (static) at α =15° where roll oscillations were observed around non-zero trim roll angle. Sectional rolling moments were calculated by integrating the upper and lower surface pressures times span-wise distance of all the measurement points from the centerline at that section. Total rolling moment C_l was estimated by integrating over all the 3 sections of the wings only as the contribution from body is negligible. It may be noticed that C_l is slightly negative at φ=0° resulting in negative φ when the model is released to FTR. Upon reaching a stable trim roll angle φ = -38° ($dC_l/d\varphi$ < 0) the roll oscillations are due to the inboard/outboard movement of suction peaks / re-attachment points on the leeward / windward wing with change in roll angle as shown in Fig. 6.

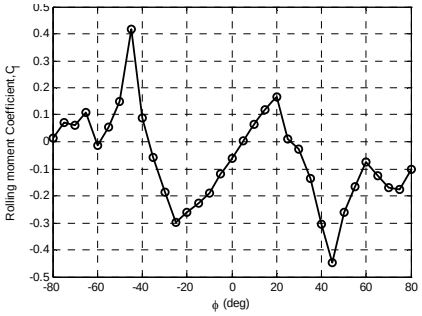

Fig. 5 Variation of C_l with static φ at α = 15°

c_p variations near the trim roll angle at x/D=4.85 and α=15° are shown in Fig. 6. This may be explained as when the model goes into negative roll the leeward wing (right) experiences an increase in the effective sweep angle and decrease in the effective α [17] resulting in the flow structure over the right wing as encountered at lower alphas (for φ=-35° α_{eff} = 12.4° and for φ=-40° α_{eff} = 11.5°). Apart from the outboard movement of suction peak on the right wing decrease in wing

surface area under suction pressure may also be noted as the model rolls from φ =-35° to -40° resulting in CW rolling moment. Another stable trim angle (φ=25°) is possible depending upon the initial roll angle. . Difference in the trim φ between Fig. 2 and Fig. 5 at α=15° is due to the different conditions; dynamic in roll in the former case contrary to static in roll in the later case. Secondly, although Forced-to-roll model (used for pressure measurements) is geometrically similar to the FTR model yet there might be minor differences due to machining or installation tolerances.

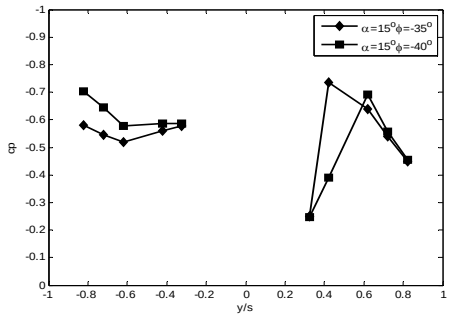

Fig. 6 c_p variations near trim roll angle at x/D=4.85 and α = 15°

3.Wings-Body Interaction Induced Roll Region

In the wings-body interaction region rolling moment is induced by the asymmetric forebody vortices, AFV, influence on the wings. Asymmetric forebody vortices patterns observed for γ in first (or 3rd) and 4th (or 2nd) quadrants were left vortex pattern (LVP) and right vortex pattern (RVP) respectively, [9]. Left vortex is lower than the right vortex in LVP and vice versa is true for RVP. Fig. 7 and Fig. 8 show static pressure distributions at φ=0°, γ=45° for various α at x/D = 3.35 (body section) and 4.85 (wing section) respectively. It may be noted that asymmetry in pressure distributions starts to develop not earlier than α= 40° & 30° at body & wing sections respectively implying that asymmetry on wings develop earlier. Also it may be noted that on the wing section (x/D=4.85) there is a little change in pressures on the left wing when α is increased from 30° to 40° contrary to the right wing where it increases with increase in α. Higher suction pressures on the outboard side of the wing towards the higher AFV are due to the effect of lower position of the wing leading edge shear layer. Higher suction pressures on the inboard side of the wing towards the higher AFV are due to the influence of higher AFV as it lies more outboard laterally from the body axis (the flow structure will be shown in para 4). The lower AFV lies more inboard laterally and has no influence on the wing towards its side. Rolling moment is induced due to this asymmetric influence of AFV on the wings. Influence of AFV on the wings change with the change in roll angle resulting in change in the upper surface rolling moment. Also the restoring (damping) moment from the lower surface starts to develop. Roll oscillations or roll-divergence is observed depending upon the magnitude of initial rolling moment and damping moment.This may be further explained by Fig. 9 which presents a typical variation of C_l in one cycle of roll oscillations. C_l in this case is determined using $C_l = \frac{I\ddot{\varphi}}{\frac{1}{2}\rho U_\infty{}^2 AS}$ where $\ddot{\varphi}$, I, A and

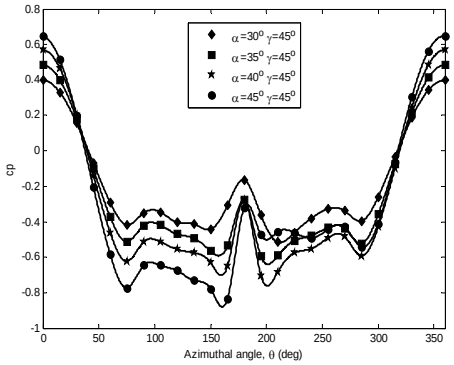

Fig. 7 Static pressure distributions at φ=0°, γ=45° for various α at x/D = 3.35 (body section)

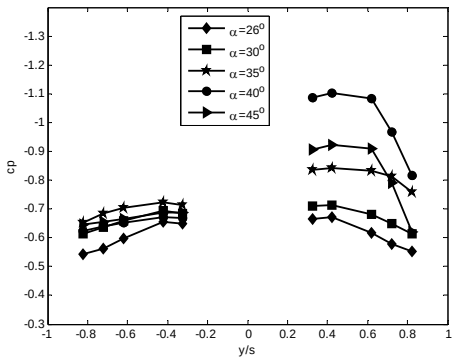

Fig. 8 Upper surface static pressure distributions at φ=0°, γ=45° for various α at x/D = 4.85 (wing section)

S are angular acceleration, moment of inertia about x axis, wings surface area and wings span respectively. In terms of energy analysis [18] clockwise loop indicates that the model absorbs energy from a mainstream while the model dissipates energy to the mainstream in the two anti-clockwise small loops. Limit cycle oscillation of a wing body is achieved owing to the equilibrium between the absorbing and dissipative energies. Dynamic unstable moment (negative damping) primarily rises from the upper surface loads which are induced by vortex systems or their interaction, and stable damping moments (positive damping) primarily is contributed by the lower surface loads which are induced by an attached flow of upwind free stream. Limit cycle, diverging or converging roll oscillations depends upon the balance between the negative and positive damping moments from the upper and lower surfaces. If the negative damping is larger than the positive one, the amplitude of oscillation will increase. If the negative damping is smaller the model oscillations will converge and stable oscillations will be established in case the two damping moments are equal.

Asymmetry in the forebody vortical flow increases with increase in angle of attack, also evident from Fig. 7, and the resulting disturbing moment also increases as a result. At earlier angles of attack in this region the damping moment overcomes the disturbing moment (as it is low) and the model

undergoes roll oscillations at negative roll trim angles. But, as the rolling moment increases ($30° \leq \alpha \leq 40°$) restoring moment could not overcome the high disturbing moment and the model goes into roll divergence.

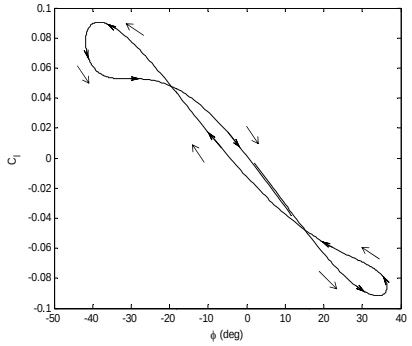

Fig. 9 Typical variation of C_l in one cycle of roll oscillation

3. Forebody Induced Roll Region

At $\alpha = 45°$, Fig. 10, higher vortex of forebody leaves the surface and new (third) vortex is generated. Forebody vortices structure changes from 2-vortices to 3-vortices at $x/D \approx 4$, [16], resulting in lowering of net rolling moment and also it is believed that there is no significant contribution from the wings flow for $\alpha > 45°$ [15]. Flow over the wings comprises of only the leading edge shear layers which is higher on the left wing for LVP and right wing for the RVP. Interaction of these forebody asymmetric vortices with wing components and their shedding downstream is responsible for the disturbing rolling moment in the forebody induced roll region. Switching of forebody asymmetric vortices pattern due to the change in the tip perturbation location during roll in addition to the damping moment provided by the lower surface (as roll angle increases) are responsible for sustaining roll oscillations.

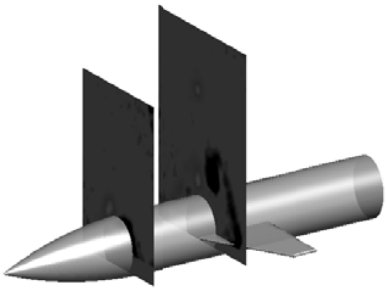

Fig. 10 Vorticity slices at x/D=2.5 & 4.35, γ=30°, α=45°, Re 0.9 10^5

4. Unsteady Effects Induced Roll Region

For $70° < \alpha \leq 90°$ the flow structure is Karman-vortex street like and is highly unsteady in nature. Small oscillations around zero mean roll angle at these alphas are due to these unsteady effects, [16].

B. Effect of Pitch Rate on Roll Behavior of FTR Model

Fig. 11 presents roll behavior of FTR model when it pitches up at various non-dimensional pitch rates. Non-dimensional pitch rate is defined as $= \omega_p L / 2U_\infty$ where ω_p, L and U_∞ represent the pitching rate in rad/s, length of the model in meters and free stream velocity in m/s respectively. Significant variation in the roll behavior occurs with increase in pitch rate. For very low pitch rates, $\leq 0.5\text{x}10^{-3}$, the behavior is very much similar to the corresponding static α behavior. Increase in , $\geq 2.5\text{x}10^{-3}$, results in suppression of any significant roll angle in the wings induced alpha region. Roll divergence phenomenon is similarly observed for dynamic cases when $\leq 2.5\text{x}10^{-3}$. Asymmetric forebody vortices dominate and control the roll motion of the model in dynamic case when $\geq 1\text{x}10^{-2}$ and there is almost no contribution to the roll motion from the wings flow in its dominance region. It may also be noted that the model's roll

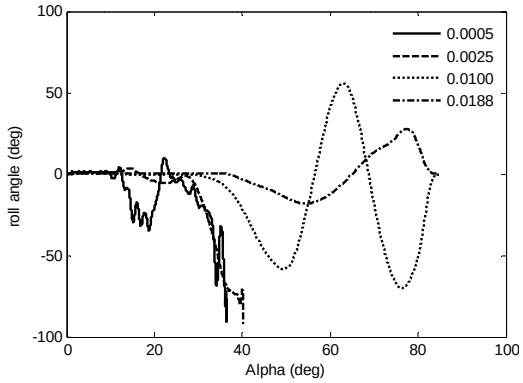

Fig. 11 Roll angle time history for FTR-pitching up model, γ=0° for various pitching speeds

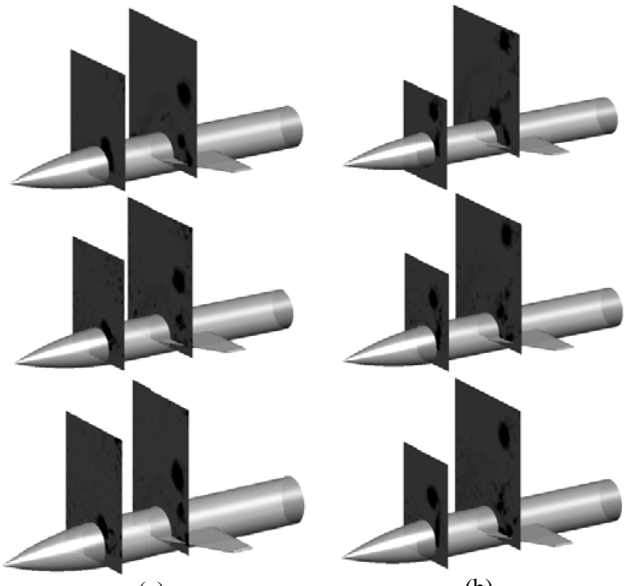

(a) (b)

Fig. 12 Vorticity contour slices at x/D=2.5 & 4.35, Re 0.9 x 10^5, γ =-30°, φ = 0° and = 0 (static), $7.5\text{x}10^{-3}$ and $1.88\text{x}10^{-2}$ [top to bottom]. a) α = 45° b) α = 52.5°

behavior follows a typical ≈ sine curve in the forebody asymmetric vortices region for $\geq 1\text{x}10^{-2}$. Increase in lag with increase in pitch rate may also be noted. Forebody asymmetric vortices structure and its variation with pitch rate at static roll angle (φ =0°) are shown in Fig. 12. Fig. 12(a)

presents vorticity slices at section x/D=2.5 and 4.35 for α = 45°, γ=-30° and Re 0.9 x 10^5 for $\bar{\omega}_p$= 0 (static), 7.5 x 10^{-3} and 1.88 x 10^{-2} from top to bottom respectively where as Fig. 12(b) presents the same information for α = 52.5°. Two trends are quite visible from these figures. Firstly, at constant pitch rate there is an increase in normal position (z-direction) of the higher vortex as angle of attack increases (viewing rows). Secondly, normal position of the higher vortex moves slightly to the lower side as pitch rate increases (viewing columns). It has also been found out (not shown here) that tip perturbation location, γ, in the first and third quadrants results in negative roll angle initially and with γ in 2nd and 4th quadrants generate positive roll angle. Detailed flow structure investigations need to be done for high pitch rates to understand the sine-curve type roll behavior at these pitching rates. Decrease in the roll amplitude with increase in pitch rate is believed to be due to weak interaction between the forebody and wing flow components as compared to the static case resulting in lower rolling moment coefficient. Fig. 13 presents the effect of pitch rate on total rolling moment coefficient at γ=45° and φ=0°. Total rolling moment is assumed to be equal to the rolling moment of the wings as contribution from body is negligible. The solid line in the figure represents static alpha-static roll (φ=0°) case. Double 'v' type behavior may be noted

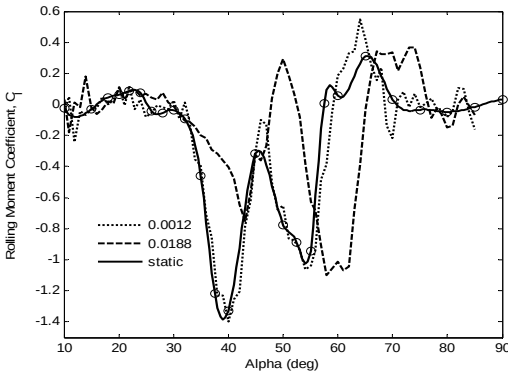

Fig. 13 Effect of pitch rate on total rolling moment coefficient, γ=45°, φ=0°

for the rolling moment coefficient. There is a decrease in the maximum value of abs(C_l) with increase in $\bar{\omega}_p$ in the first 'v' whereas there is no significant change in maximum value of second 'v'. C_l reduces to almost half as the pitch rate changes from 0 to 1.88x10^{-2} (1.31 rad/s). Change in the abs(C_l) as α increases from ≈ 40° to 45° (which is due to the change in flow structure from twin vortices to three-vortices structures) is noticed to be higher for the dynamic cases. Fig. 14 presents cp distribution at x/D=4.85 for static ($\bar{\omega}_p$=0) and dynamic ($\bar{\omega}_p$=1.88x10^{-2}) at α=40° and 42.9° respectively. These alphas correspond to the maximum $|C_l|$ encountered as shown in Fig. 13 for the two cases. It may be noticed that lower value of max$|C_l|$ for the dynamic case is due to higher suction pressures on the left wing resulting in lower $|C_l|$. Pressures on the right wing are almost same for the two cases and the higher suction pressures on the left wing for the dynamic case indicate weaker interaction between the body and wing flow components resulting in higher suction pressure and reduced $|C_l|$ as compared to the static case. Increase in windward and leeward surface pressures were observed with an increase in pitch-up rate and believed to be the main cause of sine-type motion at high pitch-up rates and roll divergence at low rates.

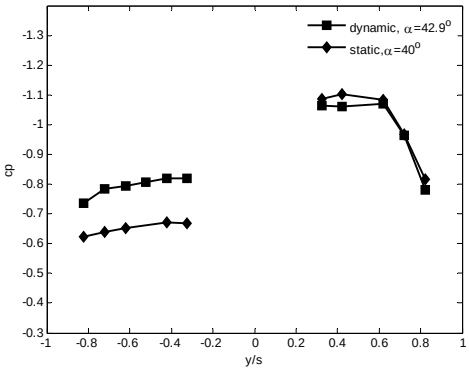

Fig. 14 Upper surface cp distributions at x/D = 4.85, γ=45°,$\bar{\omega}_p$ = 0 & 1.88x10^{-2} at α corresponding to max$|C_l|$

C. Effectiveness of the Active Control Technique for Dynamic (Pitch up) Case

Active control technique of rotating nose with artificial tip perturbation has been effectively employed in the forebody asymmetric vortices dominance alpha region, α ≥ 40° for the static case in α (no pitching), [11]. However, effectiveness of the control scheme is yet to be ascertained for the dynamic case of pitch-up and for the static case at angles of attack where the wings flow components do have an influence on the roll-oscillations.

Active control technique of rotating nose with tip perturbation is simply based on rotation of the nose tip having an artificial tip perturbation. The nose was rotated at 6 Hz which was maximum possible rotation speed of the nose motor. One complete rotation of the tip perturbation gives rise to a double square wave pattern of the side force coefficient in static case, [9]. Side force coefficient changes its direction (sign) four times per revolution of the tip. When the nose is rotated rapid switching of side force coefficient between positive and negative does not provide model sufficient time to go into large roll angles and hence is able to reduce the roll oscillations.

Effectiveness of the active control technique using rotating nose with artificial tip perturbation was investigated for wide range of angles of attack (30° to 90°) for static α-FTR and variable pitch rates for dynamic pitch-up–FTR cases. Rotational frequency of 6Hz and Re 1.6 x 10^5 was used. It has been observed in the static-α-FTR case, Fig. 15, that the active control is partially effective in the wings-body-interaction region, 30° ≤ α < 45°. It means that the control technique was able to prevent roll divergence phenomenon as observed in FTR experiments but, could not control the roll oscillations around non-zero trim roll angles in this region. Error bars show standard deviation in roll and markers indicate mean roll

angle in Fig. 15. Reasons for these roll oscillations under control need to be further investigated. However, the active control was reasonably effective in controlling the roll oscillations within few degrees in forebody-induced roll region, $40° < \alpha \leq 70°$. For the pitch-up-FTR case the active control technique was similarly able to prevent the model to go into roll divergence but, was not much effective in controlling or suppressing the roll angle as the model pitches up to higher alphas. Fig. 16 presents comparison of the roll behavior at $\bar{\omega}_p = 1.13 \times 10^{-2}$ between controlled and no-control cases. It may be noticed that the control is not very effective in this case.

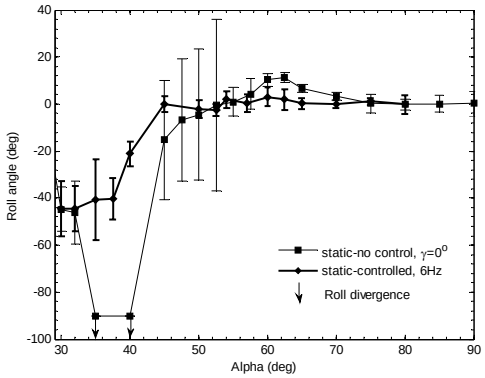

Fig. 15 Comparison of roll oscillations at static angles of attack with and without active control

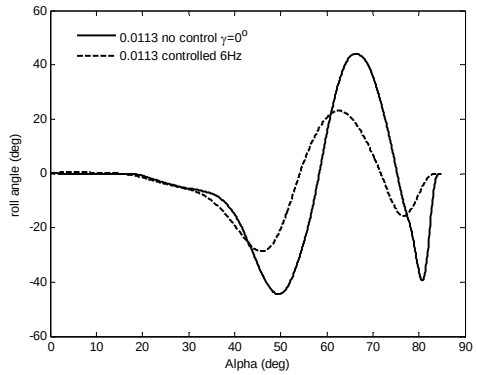

Fig. 16 Comparison of roll behavior with and without control at $\bar{\omega}_p = 1.13 \times 10^{-2}$, $\gamma=0°$

Roll angle induced in early phase of the pitching-up model (wings-induced roll region) for $\alpha_r = 0°$ reduces the effectiveness of the active control in later phase of the pitching-up motion at high alphas. α_r is the angle of attack at which the model's brake is released to set the model to FTR. However, if release of the model is delayed to $\alpha_r \geq 30°$ the active control technique is able to keep the standard deviation in roll within 10°. Table I summarizes roll angles (max & standard deviation σ_φ) in the forebody induced roll. region, $40° < \alpha \leq 70°$, for various pitch rates under active control at 6Hz for various release angles, α_r.

TABLE I
SUMMARY OF ROLL ANGLES (MAX & STD DEVIATION) FOR VARIOUS PITCH RATES UNDER CONTROL AT 6HZ FOR VARIOUS α_r

$\bar{\omega}_p$	5×10^{-4}		7.5×10^{-3}		1.88×10^{-2}	
α_r(deg)	Max $\lvert\varphi\rvert$ (deg)	σ_φ (deg)	Max $\lvert\varphi\rvert$ (deg)	σ_φ (deg)	Max $\lvert\varphi\rvert$ (deg)	σ_φ (deg)
0	24.5	6.5	34.2	19.8	11.6	3.6
30	14.3	4.6	12.8	8.4	2.8	0.9
40	12.8	4.2	5.2	2.4	1.7	0.6

REFERENCES

[1] J. Katz, "Wing / vortex interactions and wing rock". Progress in aerospace sciences 35 (1999); 727-750.
[2] R. C. Nelson, & A. Pelletier, "The unsteady aerodynamics of slender wings and aircraft undergoing large amplitude maneuvers". Progress in Aerospace Sci. 39(2003), 185-248.
[3] J. M. Brandon, and L. T. Nguyen, "Experimental study of effects of forebody geometry on high angle of attack stability". J Aircraft 1988: 25(7):591-7.
[4] T. Quast, R. C. Nelson, & D. F. Fisher. "A study of high alpha dynamic and flow visualization for 2.5% model of the F-18 HARV undergoing wing rock". AIAA Paper 91-3267.
[5] D. L. Williams II, R. C. Nelson, & D. F. Fisher. "An investigation of the X-31 roll characteristics at high angle-of-attack through subscale model testing". AIAA paper 94-0806.
[6] B. N. Pamadi, D. M. Rao, & T. Niranjana, "Wing rock and roll attractor of delta wings at high angles of attack". AIAA Paper 94-080.
[7] D. L. Williams II, R. C. Nelson. & L. E. Ericsson, "Influence of wing separation on forebody induced/driven rock". AIAA paper 95-3441-CP.
[8] T. T. Ng, C. J. Saurez, B. R. Kramer, L. Y. Ong, B. Ayers & G. N. Malcolm, "Forebody vortex control for wing rock suppression". J. Aircraft, 31, 298-305.
[9] X. Y. Deng, G. Wang, X. R. Chen, Y. K. Wang, P. Q. Liu, "Influence of nose perturbations on behaviors of asymmetric vortices over slender body". AIAA paper 2002-4710.
[10] X. Y. Deng, G. Wang, X. R. Chen, Y. K. Wang, P. Q. Liu, & Z. X. Xi, "A Physical model of asymmetric vortices flow structure in regular state over slender body at high angle of attack". Science in China (series E), 2003, 46(6): 561-573.
[11] J. Zhang, "Research on control method and mechanism of forebody vortices induced wing rock". Masters Dissertation (in Chinese), School of Aeronautical Science & Engineering, Beihang University, Beijing China, July 2010.
[12] I. Gursul, R. Gordnier, M. Visbal, "Unsteady aerodynamics of non-slender delta wings". Progress in Aerospace Sciences 41 (2005) 515–557.
[13] B. Yaniktepe, D. Rockwell, " Flow structure on a delta wing of low sweep angle". AIAA J 2004;42(3):513–23.
[14] G. Taylor, I. Gursul, "Buffeting flows over a low sweep delta wing". AIAA J 2004; 42(9):1737–45.
[15] S. C. Yen, L. C. Huang, "Flow patterns and aerodynamic performance of un-swept and swept-back wings". J. Fluids Engineering, Nov 2009, vol. 131, 111101-1-10.
[16] G. Wang, X. Y. Deng, Y.K. Wang, X. R. Chen," Zonal study of flow patterns around an ogive-cylinder at subcritical Re." J. Experiments and Measurements in Fluid Mechanics, 17(2): 19-36 (in Chinese), 2003.
[17] L. E. Ericsson, "Analysis of the Effect of Sideslip on Delta Wing Roll-Trim Characteristics", J. of Aircraft, 1997, 34 (5): 585 – 591.
[18] L. E. Nguyen, L. P. Yip, J. R. Chamber, "Self-induced wing rock of slender delta wings". AIAA Paper 81-1883